

Technical Section

Total variation diffusion and its application in shape decomposition[☆]Huayan Zhang^a, Chunxue Wang^{b,*}^aSchool of Computer Science and Technology, Tiangong University, Tianjin, China^bDunhuang Academy, Gansu, China

ARTICLE INFO

Article history:

Received 14 January 2020

Revised 5 May 2020

Accepted 6 May 2020

Available online 3 June 2020

Keywords:

Diffusion model

Total Variation

Shape segmentation

Point clouds

Augmented Lagrangian method

ABSTRACT

One challenge in shape decomposition is to capture correct boundaries between different parts and get piecewise constant results. Based on the good edge-preserving and sparsity properties of total variation regularization, this paper introduces a novel diffusion model by minimizing weighted total-variation energy with Dirichlet boundary constraints. By the total variation diffusion model, we propose an edge-preserving shape decomposition optimization model, which can be solved effectively by augmented Lagrangian method with each subproblem having closed form solution. A number of experiments display that our method can produce segmentation results with piecewise constant parts and feature-preserving boundaries for both meshes and 3D point clouds, especially for shapes with sharp features. In addition, for mesh segmentation, our results compare favorably to those obtained by several existing techniques when evaluated on the Princeton Segmentation Benchmark. Furthermore, the quantitative errors show that the algorithm is robust numerically and the computational costs are reasonable.

© 2020 Elsevier Ltd. All rights reserved.

1. Introduction

Decomposition of shapes into several semantic parts consistent with peoples' perception has become an active research topic in geometric modeling and computer graphics community. It has many applications such as parameterization, texture mapping, 3D morphing, simplification, shape retrieval, multi resolution modeling, skeleton extraction and so on.

Generally, shape segmentation involves mesh segmentation and point cloud segmentation. Wherein point clouds are usually generated by digital scanning devices, and meshes are reconstructed from scanned point clouds through triangulation methods. The main challenge for shape segmentation is to characterize where and how a shape is to be cut, and acquire the piecewise constant parts. So far a wide variety of algorithms have been developed for decomposing meshes. The interested reader can refer to an excellent survey [1], and a benchmark for evaluating mesh segmentation algorithms [2], as well as some recent developments [3–9]. With regard to 3D point cloud segmentation, readers can refer to [7].

For a smooth function Φ defined on Ω , the classical diffusion method is based on the following quadratic energy minimization

problem:

$$\min_{\Phi} \int_{\Omega} |\nabla \Phi|^2 d\Omega. \quad (1)$$

It is straightforward to derive the first order optimality condition of the problem (1) is equal to solve the following laplace equation with some boundary constraints.

$$\Delta \Phi = 0. \quad (2)$$

Due to the good property of laplace operator, various diffusion methods by discretizing laplace operator in different ways are studied, and have been successfully applied in various fields such as scientific computing [10–13,13–18], image processing [15,19–22], computer graphics [16,23–30], shape analysis [17,31–33] and so on.

In particular, laplace operator is approximately regarded as the fourier transform of 3D surfaces [34], and has been extensively applied in mesh segmentation [35–42]. The segmentation methods in [35,37] take advantage of eigenfunctions of laplace operator to project the shapes into 2-dimensional space, and finally divide the meshes according to the segmentation results of the 2-dimensional data. [38] extends the random walk method of image segmentation to mesh. Actually, the random walk method implies solving several poisson equations. [39,41] also exploit the similar manner of random walk. They first construct the feature space via solving a series of poisson equations, and then choose the suitable segmentation boundaries according to the feature space. Besides, the methods in [40,42] construct the feature space by the eigenfunctions of laplace matrix, and then cluster the feature space via the

* This article was recommended for publication by Prof H Huang.

* Corresponding Author.

E-mail addresses: zhanghy307@163.com (H. Zhang), chunxuewang2019@163.com (C. Wang).

classical Mumford-Shah model [43], which can also optimize the boundaries between different parts.

Overall, these segmentation methods all take advantage of the laplace operator, which is closely related to the diffusion energy (1). As known, laplace operator is second order differentiable, and the diffusion energy (1) is very smooth. It is quite difficult to capture the segmentation boundaries and get the piecewise constant parts. Therefore, the segmentation methods based on laplace operator always fail in producing results with better boundaries. This situation is more severe for CAD meshes and 3D point clouds. In addition, most of existing segmentation methods involve several steps such as: first constructing feature spaces according to laplace equation or eigenfunction, then devising greedy optimization algorithms to cluster each parts, and finally trying to optimize segmentation boundaries. These steps complicate the algorithm.

Motivated by the good edge-preserving and sparse(ℓ_1 – norm) property of total variation regularization [44] and its extensions [45–49], which have been widely used in image restoration and segmentation problems, we investigate the following total variation diffusion energy to devise a novel shape segmentation method:

$$\min_{\Phi} \int_{\Omega} |\nabla \Phi| d\Omega, \quad (3)$$

which is equal to solve the following nonlinear diffusion equation with some boundary constraints.

$$\operatorname{div}(\nabla \Phi / |\nabla \Phi|) = 0. \quad (4)$$

Actually, the above problem (4) has been studied for feature-preserving signal processing. As the discretization of the nonlinear diffusion equation (4) is not accurate(which is essentially a discrete form of Laplace operator, that is weighted equation of (2)): $\Delta_w \Phi = 0$, its diffusion solutions are not always equal to that of (3). By contrast, in the paper, we focus on devising diffusion algorithms by solving problem (3) directly.

In the paper, different from many existing segmentation methods based on the classical diffusion energy (1), we devote to studying the total variation diffusion model (3) and its application in shape segmentation. By giving definitions of the gradient operator (3) by piecewise constant basis(see [49]) on meshes and point clouds respectively, we construct two weighted total variation norms. With the two norms, we propose a weighted total variation diffusion shape decomposition method, which is quite simple and no need for further relaxations. Besides, we employ augmented Lagrangian method (ALM) [48,49] to effectively solve the non-differentiable problem. Numerous experiments show that this total variation diffusion shape segmentation method works well for both meshes and 3D point clouds. The quantitatively errors also show that the algorithm is robust numerically and the computational costs are reasonable. Moreover, when compared to several existing approaches including evaluated on the benchmark set [2] and pointnet set [50], it always gives better segmentation results with piecewise constant parts, which is consistently with human perception.

The paper is organized as follows: Section 2 gives some notations, definitions of gradient operator and total variation diffusion model. In Section 3, we introduce our total variation diffusion shape decomposition method. Section 4 describes the details of the algorithm for solving our total variation diffusion shape segmentation problem. In Section 5, we provide numerical experiments. Section 6 concludes the paper.

2. Notations and total variation diffusion model

In this section, we first briefly give some notations, and then introduce weighted total variation (WTV) norms, and finally present our total variation diffusion model.

2.1. Notations

Without loss of generality, we denote a discrete 3D shape as S , which includes point cloud $C \subset \mathbb{R}^3$ and triangulated mesh $M \subset \mathbb{R}^3$. As point cloud C does not have topological connection, we construct its k neighbors by kNN(k-Nearest Neighbour) method. The vertices and edges of point cloud C are denoted as $\{v_i : i = 0, 1, \dots, V_C - 1\}$ and $\{e_i : i = 0, 1, \dots, E_C - 1\}$. V_C and E_C are the numbers of vertices and edges. For triangulated mesh M with no degenerate triangles, the set of vertices, edges and triangles of M are denoted as $\{v_i : i = 0, 1, \dots, V_M - 1\}$, and $\{e_i : i = 0, 1, \dots, E_M - 1\}$, and $\{\tau_i : i = 0, 1, \dots, T_M - 1\}$. Here V_M , E_M and T_M are the numbers of vertices, edges and triangles, respectively. If v is an endpoint of an edge e , then we denote it as $v \prec e$. Similarly, if τ is a triangle of an edge e , it is denoted as $\tau \prec e$; For each edge e , we choose a direction arbitrarily. If the direction of e is consistent with its connecting triangle τ , we denote $\operatorname{sgn}(\tau, e) = 1$, else $\operatorname{sgn}(\tau, e) = -1$. Similarly, for the endpoints v_i, v_j of an edge e , $\bar{v}_i \bar{v}_j$ is viewed as the direction of v_i . If the direction of v_i is the same as edge e , we denote $\operatorname{sgn}(v_i, e) = 1$, else $\operatorname{sgn}(v_i, e) = -1$.

2.2. The definitions of gradient operators and weighted total variation norms for S

As our method involves both triangulated mesh and 3D point cloud, we first present the definitions of gradient operator on both type data. To acquire the piecewise constant diffusion results, we discretize the gradient operators by the piecewise constant basis(see [49]).

For vector $\mathbf{u} = (\mathbf{u}_0, \dots, \mathbf{u}_\tau, \dots, \mathbf{u}_{T_M-1}) \in R^{T_M \times n}$ defined on M and $\mathbf{p} = (\mathbf{p}_0, \dots, \mathbf{p}_v, \dots, \mathbf{p}_{V_C-1}) \in R^{V_C \times n}$ defined on C . That is $\mathbf{u}_\tau = (u_{\tau,1}, \dots, u_{\tau,n})$ and $\mathbf{p}_v = (p_{v,1}, \dots, p_{v,n})$ are n -dimensional vector on triangle τ and vertex v respectively. Similar to [49], for each edge e , the gradient operators on M and C have the following forms:

$$\nabla_M : \nabla_M \mathbf{u}|_e = \begin{cases} \sum_{\tau \prec e} \mathbf{u}_\tau \operatorname{sgn}(\tau, e), & e \not\subseteq \partial M \\ 0, & e \subseteq \partial M \end{cases} \quad (5)$$

$$\nabla_C : \nabla_C \mathbf{p}|_e = \sum_{v \prec e} \mathbf{p}_v \operatorname{sgn}(v, e) \quad (6)$$

Based on the gradient operators (5) and (6), for \mathbf{u} and \mathbf{p} , we define the following weighted total variation norms for M and C respectively.

$$R_{\text{wtv}}(\nabla_M \mathbf{u}) = \text{TV}_M(\mathbf{u}) = \|\nabla_M \mathbf{u}\|_1 = \sum_e \left(\sum_{i=1}^n |(\nabla_M \mathbf{u}|_e)_i| \right) w_{e,M} l_e \quad (7)$$

$$R_{\text{wtv}}(\nabla_C \mathbf{p}) = \text{TV}_C(\mathbf{p}) = \|\nabla_C \mathbf{p}\|_1 = \sum_e \left(\sum_{i=1}^n |(\nabla_C \mathbf{p}|_e)_i| \right) w_{e,C} l_e \quad (8)$$

where l_e denoting the length of edge e , $w_{e,M}$ and $w_{e,C}$ are determined by the difference between triangle normals and vertex normals of edge e respectively; see Section 5.1 for details.

According to weighted total variation norms defined in (7) and (8), we introduce the following total variation diffusion model on triangulated mesh M and point cloud C respectively.

Ramrak 1. For convenience, we unified TV_M and TV_C as TV , ∇_M and ∇_C as ∇_S , $w_{e,M}$ and $w_{e,C}$ as w_e .

2.3. The total variation diffusion model

We discretize the continuous nonlinear energy (3) by weighted total variation norms defined in (7) and (8), and get the following total variation diffusion optimization problem with Dirichlet

boundary constraint:

$$\begin{aligned} \min_{\Phi} \int_S |\nabla_S \Phi| d\Omega &= \min_{\Phi} R_{\text{wtv}}(\nabla_S \Phi), \\ \text{s.t. } \Phi|_{\partial S} &= \Phi^{\text{in}}. \end{aligned} \quad (9)$$

In the following, we focus on applying this total variation diffusion model in shape decomposition, which includes triangulated mesh and point cloud data respectively.

3. Shape decomposition using total variation diffusion model

Shape decomposition aims to divide a given discrete shape S into K piecewise smooth regions: $S_1, S_2, \dots, S_k, \dots, S_K$ with the K parts satisfying: $S_i \cap S_j = \emptyset, i \neq j$ and $\bigcup_{i=1}^K S_i = S$. For shape segmentation problem, smooth and clear segmentation boundaries are very important for downstream geometry applications. Most existing segmentation methods usually involve several steps: first introducing feature spaces according to laplace operator, then devising greed optimization algorithm to cluster each parts, and finally optimizing segmentation boundaries [7,38,40,42]. Different from most existing segmentation methods, by the good edge-preserving and sparsity property of total variation regularization, we propose the following one-stage total variation diffusion shape decomposition method, which can always achieve piecewise constant diffusion results with edge-preserving boundaries.

Specifically, for $\Phi = (\Phi_0, \dots, \Phi_i, \dots, \Phi_{N_S-1}) (N_S = T_M \text{ for meshes}, N_S = V_C \text{ for point clouds})$ with $\Phi_i = (\Phi_{i,1}, \dots, \Phi_{i,K})$ being K -dimensional vector, we have the following shape decomposition model:

$$\begin{aligned} \min_{\Phi \in \mathcal{O}} E(\Phi) &= R_{\text{wtv}}(\nabla_S \Phi), \\ \text{s.t. } \Phi|_{\partial S} &= \Phi^{\text{in}}, \end{aligned} \quad (10)$$

where ∂S is consisting of K given seeds $\{s_1, s_2, \dots, s_K\}$, the value of Φ^{in} being 0 or 1, and $\mathcal{O} = \{\Phi_i = (\Phi_{i,1}, \dots, \Phi_{i,k}, \dots, \Phi_{i,K}) : \Phi_{i,k} \geq 0, \sum_{k=1}^K \Phi_{i,k} = 1, \forall i\}$ indicates the connectivity of each segmenting part.

Specifically, by introducing the following function:

$$\chi(\Phi) = \begin{cases} 0, & \Phi \in \mathcal{O} \\ +\infty, & \Phi \notin \mathcal{O}, \end{cases} \quad (11)$$

the above problem (10) can be reformulated as follows:

$$\begin{aligned} \min_{\Phi} R_{\text{wtv}}(\nabla_S \Phi) + \chi(\Phi) \\ \text{s.t. } \Phi_{S_i,k} = \delta_{i,k}, i = 1, \dots, K, \\ k = 1, \dots, K. \end{aligned} \quad (12)$$

where $\delta_{i,k}$ is the following dirac delta function:

$$\delta_{i,k} = \begin{cases} 1, & i = k, \\ 0, & i \neq k. \end{cases}$$

4. Augmented Lagrangian method(ALM) for solving (12)

As the total variation term is non-differentiable, we propose to solve our shape segmentation problem(12) by augmented Lagrangian method(ALM)[48,49].

By introducing two auxiliary variables \mathbf{q} and \mathbf{z} , we reformulate (12) to be the following equality constrained problem:

$$\begin{aligned} \min_{\Phi, \mathbf{q}, \mathbf{z}} R_{\text{wtv}}(\mathbf{q}) + \chi(\mathbf{z}), \\ \text{s.t. } \mathbf{q} = \nabla_S \Phi, \mathbf{z} = \Phi, \Phi_{S_i,k} = \delta_{i,k}, i = 1, \dots, K, \\ k = 1, \dots, K. \end{aligned} \quad (13)$$

In order to solve (13), we define the following augmented Lagrangian functional

$$L(\Phi, \mathbf{q}, \mathbf{z}; \lambda_{\mathbf{q}}, \lambda_{\mathbf{z}}) = R_{\text{wtv}}(\mathbf{q}) + \chi(\mathbf{z}) + \langle \lambda_{\mathbf{z}}, \mathbf{z} - \Phi \rangle$$

$$\begin{aligned} &+ \frac{r_z}{2} \|\mathbf{z} - \Phi\|^2 + \langle \lambda_{\mathbf{q}}, \mathbf{q} - \nabla_S \Phi \rangle \\ &+ \frac{r_{\mathbf{q}}}{2} \|\mathbf{q} - \nabla_S \Phi\|^2 \end{aligned} \quad (14)$$

It has been demonstrated that the solution of equation (13) is equivalent to that of the following saddle-point problem with constraints:

$$\max_{\lambda_{\mathbf{q}}, \lambda_{\mathbf{z}}} \min_{\Phi, \mathbf{q}, \mathbf{z}} L(\Phi, \mathbf{q}, \mathbf{z}; \lambda_{\mathbf{q}}, \lambda_{\mathbf{z}}), \quad (15)$$

We then iteratively solve the saddle-point problem by separating (14) into the following three subproblems:

- The Φ -sub problem:

$$\begin{aligned} \min_{\Phi} & \frac{r_{\mathbf{q}}}{2} \|\nabla_S \Phi - (\mathbf{q} + \frac{\lambda_{\mathbf{q}}}{r_{\mathbf{q}}})\|^2 + \frac{r_z}{2} \|\Phi - (\mathbf{z} + \frac{\lambda_{\mathbf{z}}}{r_z})\|^2 \\ \text{s.t. } & \Phi_{S_i,k} = \delta_{i,k}, i = 1, \dots, K, \\ & k = 1, \dots, K. \end{aligned} \quad (16)$$

This quadratic problem with constraints can be directly solved by various numerical packages, such as MKL, Taucs and Eigen.

- The \mathbf{q} -sub problem:

$$\min_{\mathbf{q}} R_{\text{wtv}}(\mathbf{q}) + \langle \lambda_{\mathbf{q}}, \mathbf{q} \rangle + \frac{r_{\mathbf{q}}}{2} \|\mathbf{q} - \nabla_S \Phi\|^2, \quad (17)$$

which has the following closed form solution [48,49].

$$\mathbf{q}_{e,k} = \begin{cases} (1 - \frac{w_e}{r_{\mathbf{q}}|\mathbf{W}_{e,k}|})\mathbf{W}_{e,k}, & |\mathbf{W}_{e,k}| > \frac{w_e}{r_{\mathbf{q}}}, \\ 0, & |\mathbf{W}_{e,k}| \leq \frac{w_e}{r_{\mathbf{q}}}, \end{cases} \quad (18)$$

where

$$\mathbf{W}_{e,k} = \nabla_M \Phi_{e,k} - \frac{\lambda_{\mathbf{q}} \cdot \mathbf{q}}{r_{\mathbf{q}}}.$$

- The \mathbf{z} -sub problem:

$$\min_{\mathbf{z}} \chi(\mathbf{z}) + \langle \lambda_{\mathbf{z}}, \mathbf{z} \rangle + \frac{r_z}{2} \|\mathbf{z} - \Phi\|^2, \quad (19)$$

which can be calculated via Michelot's algorithm [51].

The algorithm for solving (13) is listed in Algorithm 1.

Ramrak 2. Due to the non strictly convex of total variation regularization, the solution is not unique, while we have the following convergence analysis by [48,52]:

The sequence $\{(\Phi^n, \mathbf{q}^n, \mathbf{z}^n)\}$ generated by the alternating minimization has cluster points. Any cluster point is a partial optimum of $L(\Phi, \mathbf{q}, \mathbf{z}; \lambda_{\mathbf{q}}^n, \lambda_{\mathbf{z}}^n)$.

5. Experimental results and discussions

In this section, we present numerical experiments with total variation diffusion method for triangulated mesh segmentation and 3D point cloud segmentation respectively. We implement our method by Microsoft Visual Studio 2010. All the examples are tested on a laptop with Intel Corei7 and 8GB RAM. To demonstrate the effectiveness and robustness of our method, we discuss our algorithm from several aspects, such as parameters, noise, numerical error, comparisons both quantitatively and visually to several typical existing methods. In particular, we compare our method with classical diffusion method (1) (The classical diffusion method indicates segmentation methods based on Laplace operator, which is implemented by solving (12) with $\|\nabla_S \Phi\|_2^2$ norm. For convenience, we abbreviate our method and the classical diffusion method as "TV-based" and "Laplace-based").

Besides, for mesh segmentation, we tested our segmentation results on the Princeton Segmentation Benchmark [2], which contains 19 categories of 380 meshes, human segmentation results,

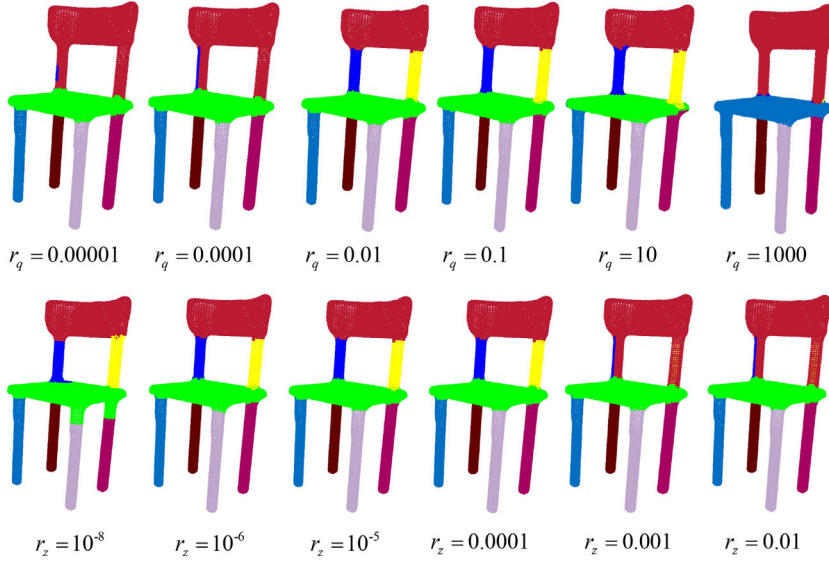


Fig. 1. Segmentation results with different r_q , r_z for point data. The first row presents results with different r_q for fixed $r_z = 10^{-4}$; the second row shows results with different r_z with fixed $r_q = 0.01$.

and code for evaluating segmentation methods. With this benchmark, we also compare our approach both quantitatively and visually to several typical existing methods, including Rand Cuts [4], Shape Diam [53], Random Walks [38], Isoline Cut [39], WCseg [7], S-MS 2018[42] and two learning-based methods SB19 2010[5] and PCN12 2017[8]. Their segmentation results are provided by Princeton Segmentation Benchmark [2] or the authors.

In addition, for point cloud segmentation, we compare with “WCseg”[7](the results of [7] are downloaded from their project homepage). Most data tested in the paper are from the benchmark set [2] and pointnet set [50]. In addition to the two data sets, we also tested our algorithm on more meshes (such as Fig. 4 and Fig. 9).

5.1. Parameters

In our algorithm, there are two algorithm parameters r_q , r_z . As the two parameters are from augmented Lagrangian method, data type and data size have a low impact on them. According to our experiment, r_q is larger than r_z , and we cannot get satisfying results when two parameters are too large or too small. By our tests, they can be fixed by $r_q = 0.01$ and $r_z = 0.0001$. Fig. 1 presents segmentation results with different r_q for fixed r_z (the first row) and different r_z for fixed r_q (the second row) respectively.

Besides, the weights $w_{e,M}$ and $w_{e,C}$ play an important role in identifying sharp edges in our shape decomposition method, which are defined as

- (a) For triangulated mesh segmentation, to better describe the sharp edges of a surface, $w_{e,M}$ is measured by the gauss kernel of the difference between triangle normal $\mathbf{N}_{\tau_i}, \mathbf{N}_{\tau_j}$ across edge e ,

$$w_{e,M} = e^{-\frac{\|\mathbf{N}_{\tau_i} - \mathbf{N}_{\tau_j}\|^2}{\sigma_1^2}}, \quad (20)$$

where σ_1 is the average of triangle normal difference over all edges.

- (b) For point cloud segmentation, as the point clouds do not have topological connections, for each point v_i , we first construct its k neighborhood by k-Nearest Neighbor (kNN) algorithm. Then, we estimate normal \mathbf{n}_i of each point v_i via the classical principal components analysis (PCA). The $w_{e,C}$ is finally defined by the gauss kernel of the difference between

end point normal $\mathbf{n}_i, \mathbf{n}_j$ of edge e :

$$w_{e,C} = e^{-\frac{\|\mathbf{n}_i - \mathbf{n}_j\|^2}{0.01\sigma_2^2}}, \quad (21)$$

where σ_2 is the average of point normal similarity over all edges.

- (c) Furthermore, for parameter k in kNN algorithm, by our tests, 10 is an empirical value. To demonstrate the effectiveness of the empirical value k in (kNN) algorithm, we present segmentation results with different k in Fig. 2.
(d) Fig. 3 shows diffusion results with $w_e = 1$ (the first row) and w_e defined by (20) and (21) (the second row) respectively. We can see that both the results can get the piecewise constant segmentation parts. However, the results with weights defined by (20) and (21) can preserve feature boundaries between different parts. By contrast, the results with $w_e = 1$ fail in capturing the boundaries between head and body of the bear mesh.

5.2. Application for triangulated surface segmentation

The laplace operator derived from classical diffusion (1) has been successfully applied in triangulated mesh segmentation [4,35,37–42]. However, as the laplace operator is second order differential operator, its solutions are very smooth. For a surface with sharp features, it is difficult to describe these features and cannot produce piecewise constant results.

In Fig. 4, for the same initializations and the weight $w_{e,M}$, we show diffusion results and corresponding segmentation results for triangulated meshes with many sharp edges by total variation diffusion and classical diffusion model (1) respectively. As shown, the diffusion results with (1) are not able to distinguish shallow edges from smooth regions(see the results in the rectangular box with the rows marked by “Laplace-based”). Therefore, the final segmentation results (see the column marked by “SegResult” with rows marked by “Laplace-based”) are unsatisfactory. By contrast, the diffusion results by total variation diffusion model are piecewise constant, and can effectively identify these shallow edges (see the results in the rectangular box with rows marked by “TV-based”). The final segmentation results are very satisfying and feature-preserving(see the column marked by “SegResult” with rows marked by “TV-based”).

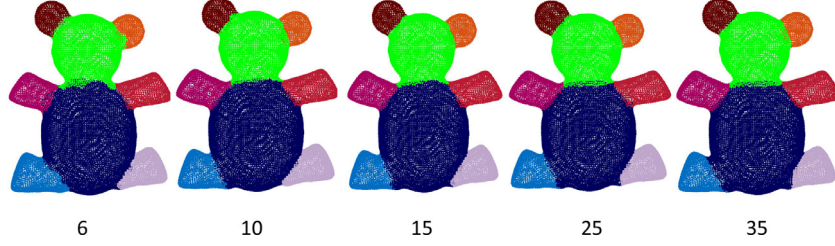


Fig. 2. Comparison of segmentation results with different k in kNN algorithm.

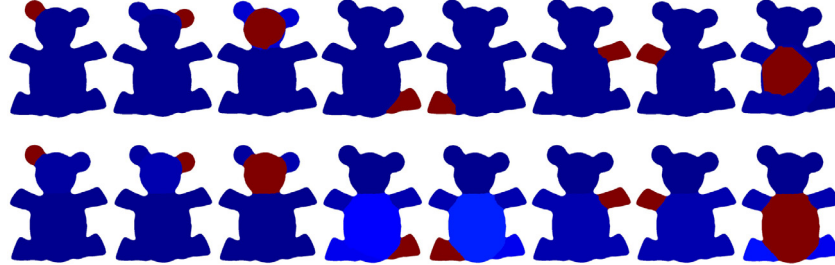


Fig. 3. Comparison of diffusion results with $w_e = 1$ (the first row) and w_e given by (20) and (21) (the second row).

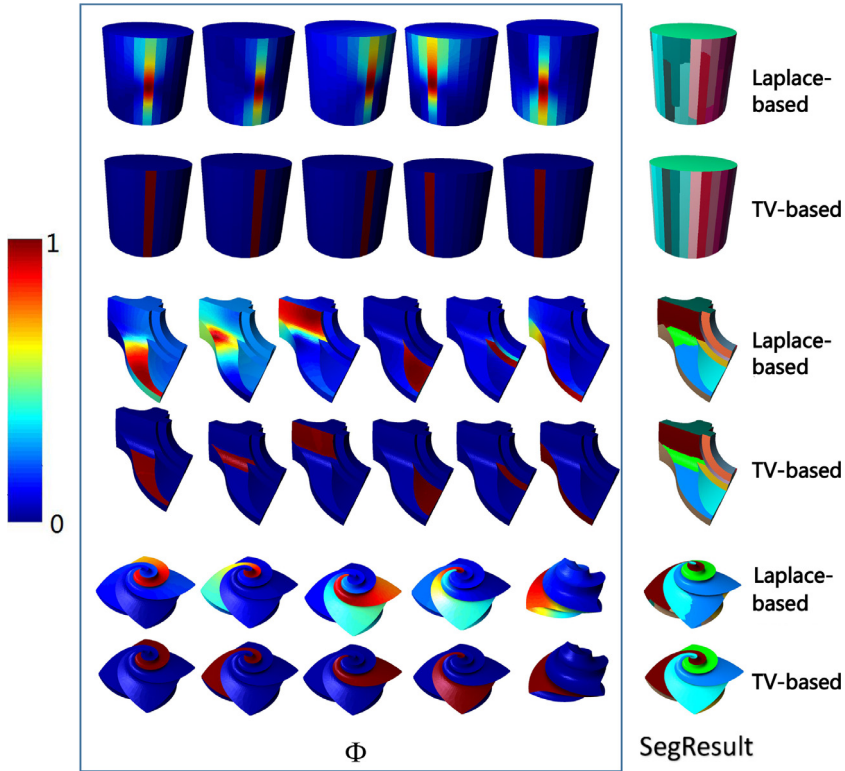


Fig. 4. Comparison of diffusion results and segmentation results by classical diffusion model and total variation diffusion model for CAD meshes.

Besides, we also test the two methods on smooth meshes in Fig. 5. For this type meshes, both methods can give well segmentation results. However, the diffusion results with total variation diffusion method are piecewise constant with clear boundaries, while the solutions with classical diffusion model are smooth and the boundaries are not clear. Therefore, the final segmentation boundaries with total variation diffusion model are better than those of (1); see the segmentation boundaries of the two meshes (the column marked by “SegResult”).

To further demonstrate the effectiveness of total variation diffusion method, we present more comparisons in Fig. 6, which illustrates that the results with total variation diffusion method are

better than those of the classical diffusion method both for CAD and non-CAD meshes, especially for CAD meshes.

Finally, we present evaluation results on benchmark data sets in [2]. Fig. 7 shows the quantitative comparisons between our method and other methods according to the four error metrics in [2] (Cut Discrepancy (“CD”), Hamming Distance-missing rate/false alarm rate (“Hamming-Rm/Rf”), Rand Index (“RI”) and Global/Local Consistency Error (“G/LCE”)). We can see that our results have lower errors than other methods except deep learning based method PCN12 2017[8]. More details on the Rand Index metric are shown in Table 1, where the Rand Index scores of all the compared methods for the 19 categories of meshes in Princeton Seg-

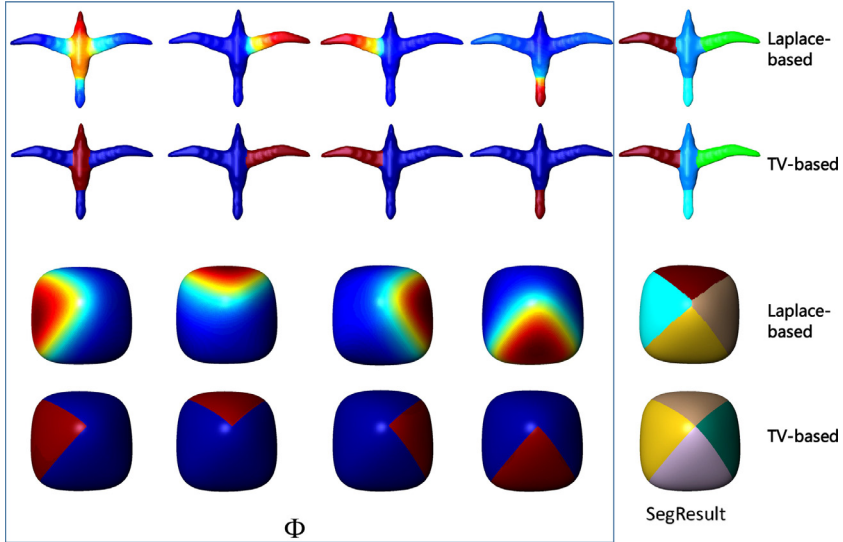


Fig. 5. Comparison of diffusion results and segmentation results by classical diffusion model and total variation diffusion model for smooth meshes.

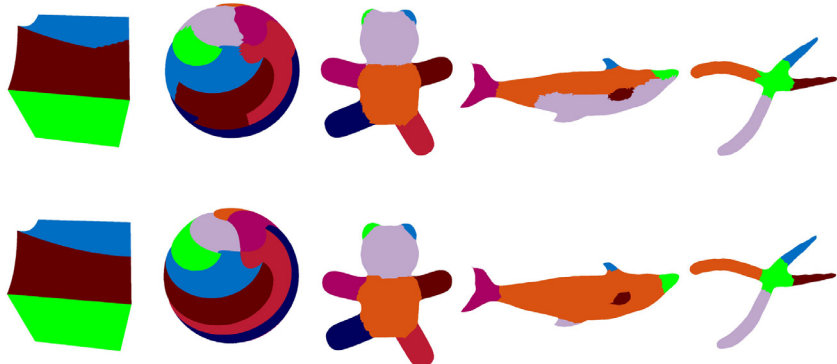


Fig. 6. Comparison of segmentation results by classical diffusion model (first row) and total variation diffusion model (second row) for more meshes.

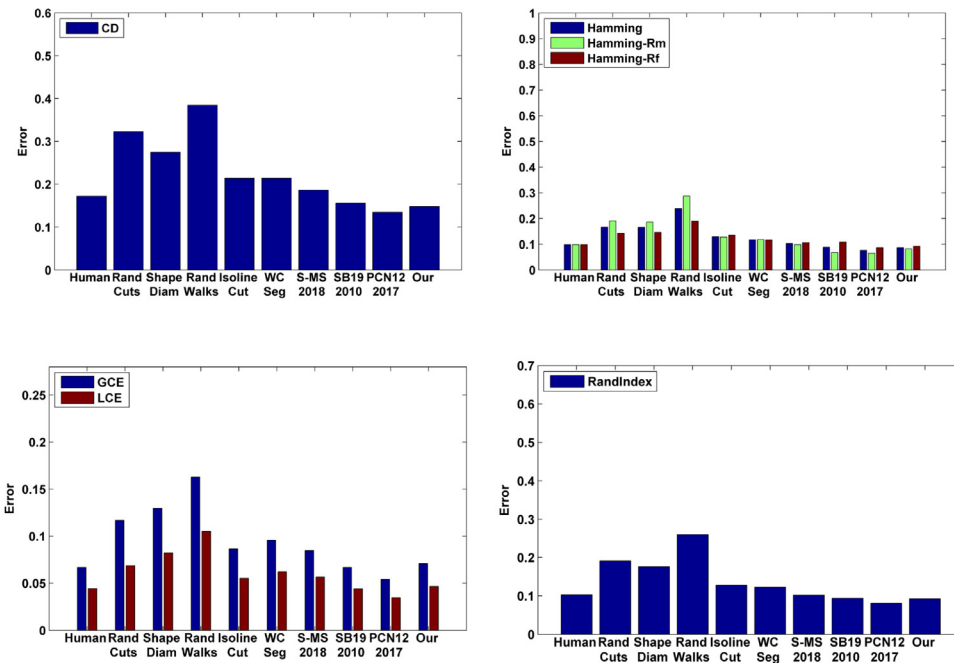


Fig. 7. Evaluation of segmentation in terms of four evaluation metrics. The evaluations are performed according to the protocols and human segmentations in the Princeton Segmentation Benchmark of [2].

Table 1

Rand Index scores(the smaller the value, the better the segmentation results) across all 19 categories using our method and previous methods based on the Princeton Segmentation Benchmark of [2].

Categories	Human	Rand cuts	Shape Diam	Rand Walks	Isoline Cut	WC Seg	SMS 2018	SB19 2010	PSN12 2017	Our
Human	13.5	13.1	17.9	21.9	12.3	12.8	12.9	11.9	11.2	12.2
Cup	13.6	21.9	35.8	35.8	21.	17.1	10.6	10	9.9	9.5
Glasses	10.1	10.11	20.4	31.1	9.8	17.3	9.5	13.6	8.3	9.7
Airplane	9.2	12.18	9.2	24.8	12.7	8.9	10.0	7.8	7.3	9.0
Ant	3.0	2.5	2.2	6.8	3.9	2.1	2.1	1.8	1.7	1.9
Chair	8.9	18.3	11.1	15.6	12.1	10.3	6.8	5.4	5.2	5.7
Octopus	2.4	6.3	4.5	6.7	4.1	2.9	2.4	1.9	1.8	2
Table	9.3	38.2	18.4	13.1	6.5	9.1	6.6	5.6	6	7.8
Teddy	4.9	4.5	5.7	12.7	5.3	5.6	3.6	3.2	3.1	3.7
Hand	9.1	8.9	20.2	18.9	11.5	11.6	7.8	10.4	9.1	8.6
Plier	7.1	10.9	37.5	23.0	7.3	8.7	8.7	5.3	5	7.6
Fish	15.5	29.6	24.8	38.8	24.3	20.3	21.8	12.8	11.7	13.4
Bird	6.2	10.7	11.5	24.9	9.7	10.1	7.3	8.8	4.4	9.1
Armadillo	8.3	9.2	9.0	11.5	10.6	8.1	9.5	7	6.3	8.6
Bust	22.0	23.2	29.8	29.8	24.4	26.5	24.8	23.8	18.8	22.5
Mech	13.1	27.7	23.8	21.1	12.2	18.2	11.2	11	8.6	9.3
Bearing	10.4	12.3	11.9	24.6	17.7	11.9	9.2	9.1	12.9	8.6
Vase	14.4	13.3	23.9	24.5	16.8	16.1	11.9	14.7	10.5	12.2
FourLeg	14.9	17.4	16.1	21.8	18.1	15.2	15.6	13.9	11.6	14.8
Average	10.3	15.3	17.6	21.5	12.7	12.3	11.0	9.37	8.1	9.27

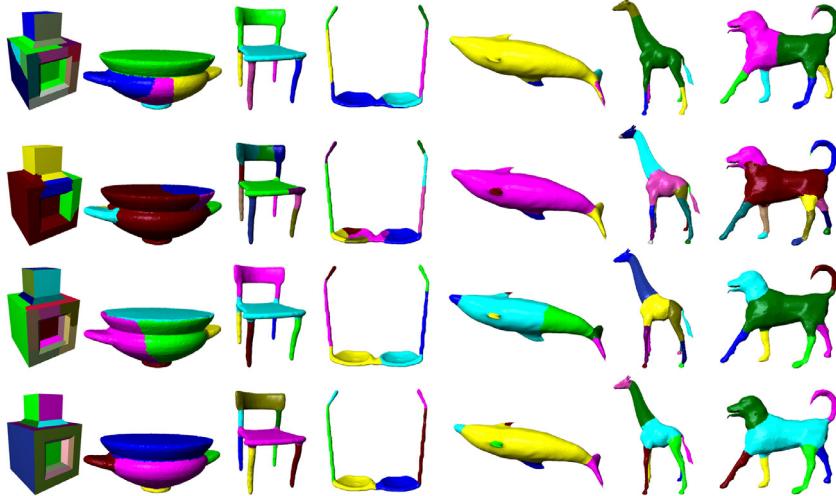


Fig. 8. Comparison of segmentation results by RandWalk(first row), WCSeg(second row), S-MS 2018(third row) and our total variation diffusion model (fourth row).

mentation Benchmark are listed. Fig. 8 presents visually the comparison on segmentation results between our method and other three methods. One can observe the results with our method can capture more correct boundaries than those of other three methods, which either fails in capturing the boundaries or over cutted.

Anyhow, our total variation diffusion segmentation method can produce effective segmentation results both for CAD meshes and non-CAD meshes.

5.3. Application for 3D point cloud decomposition

Segmenting scanned 3D point clouds can greatly simplify the subsequent analysis and reconstruction. Due to lack of topology information, it is quite difficult to capture the feature parts. Most existing point cloud segmentation methods focus on large scenes segmentation [54–56]. For single shape, readers can refer to [7]. In the paper, we only consider single shape segmentation. Based on the good edge-preserving and sparsity property of total variation norms, we propose to apply total variation diffusion model for segmenting 3d point cloud shapes.

We first test our algorithm on two synthetic data in Fig. 9, and show the diffusion results and corresponding segmentation results by total variation diffusion and diffusion model (1) re-

spectively. Note that the total variation diffusion results are quite piecewise constant and capture the boundaries of each parts correctly (see the results in the rectangular box with rows marked by “TV-based”). Consequently, the corresponding segmentation results are consistent with human perception (see the column marked by “SegResult” with rows marked “TV-based”). Nevertheless, the diffusion results with (1) are quite smooth and fail in preserving the boundaries of each parts (see the results in the rectangular box with rows marked by “Laplace-based”), and the segmentation results by (1) are not well (see the column marked by “SegResult” with rows marked “Laplace-based”).

In Fig. 10, for the same initializations and weight $w_{e,M}$, we show results for 3d point cloud shapes from benchmark set [2] by total variation diffusion and classical diffusion model (1) respectively. Similarly, the diffusion results with classical diffusion model are very smooth, and unable to distinguish feature parts from each other (see the results in the rectangular box with rows marked by “Laplace-based”). Therefore, the final segmentation results (see the column marked by “SegResult” with rows marked “Laplace-based”) are not well. By contrast, the diffusion results by total variation diffusion model can effectively identify these parts with very piecewise constant solutions (see the results in the rectangular box with rows marked by “TV-based”), and the final segmentation results

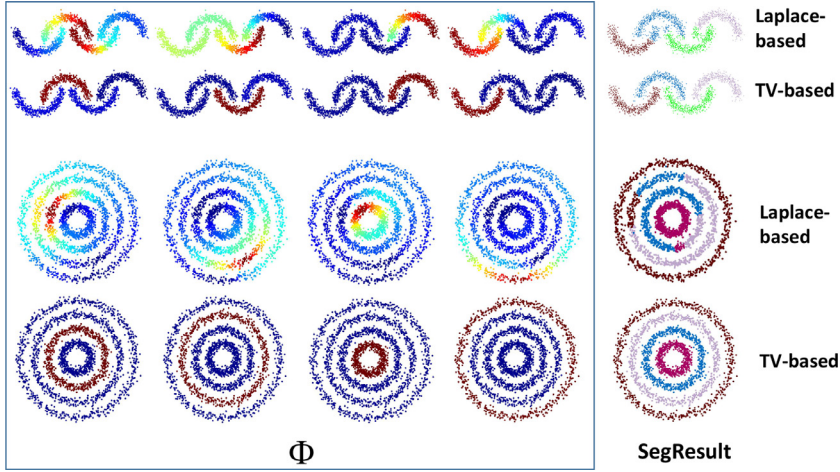


Fig. 9. Comparison of diffusion results between classical diffusion model and total variation diffusion model for synthetic data.

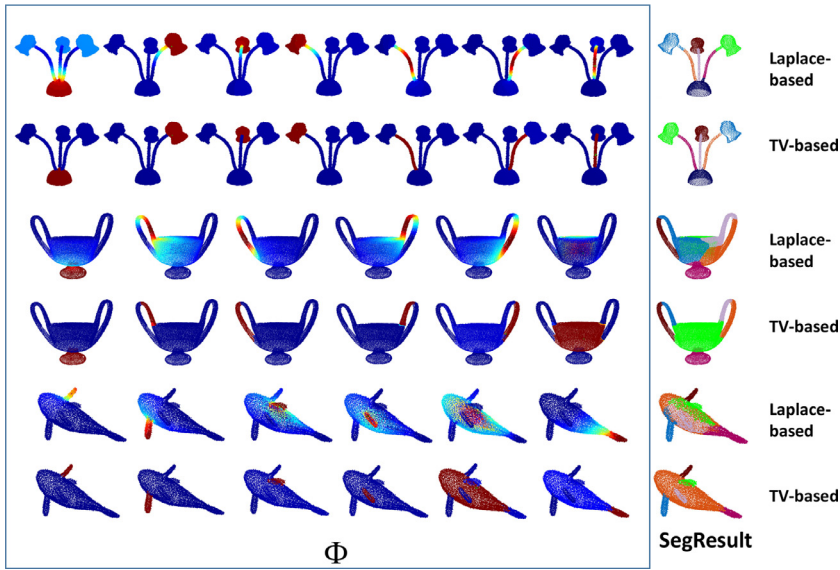


Fig. 10. Comparison of diffusion results between classical diffusion model and total variation diffusion model for 3d point cloud data.

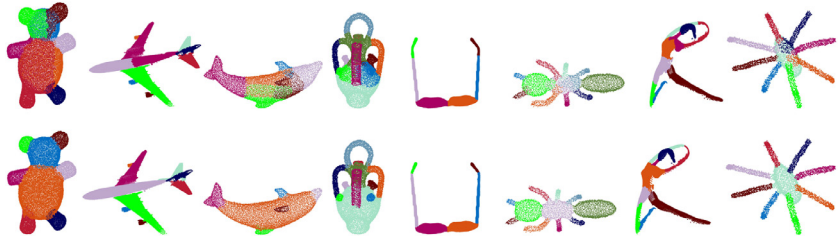


Fig. 11. Comparison of segmentation results with classical diffusion model(first row) and total variation diffusion model(second row) for more 3d point clouds.

are very boundary preserving(see the column marked by “SegResult” with rows marked by “TV-based”).

In addition, we present more comparable results in Fig. 11, which further prove that our method can produce solutions with boundary-preserving and piecewise constant parts. However, the solutions with classical diffusion model are smooth and the boundaries are not well. We also compare our total variation diffusion method with that in [7] in Fig. 12, which show that the results by [7] and the diffusion (1) are either failing in capturing the boundaries or over-segmented. By comparison, the results by our method are satisfying and preserving segmenting boundaries.

Besides, we test our algorithm on Pointnet data set [50]. In Fig. 13, we present comparative results between the ground-truth(the first row, used for training in [50]) and our segmentation results(the second row), and the corresponding difference maps are shown in the third row. As can be seen our results are almost consistent with the ground-truth. More segmentation results on the Pointnet dataset [50] are exhibited in Fig. 14. Furthermore, we present segmentation results for more 3d point clouds in Fig. 15. Overall, total variation diffusion segmentation method can get edge-preserving results.

Finally, to further demonstrate the effectiveness of our algorithm, in Fig. 16, we test our algorithm on data with noise at dif-

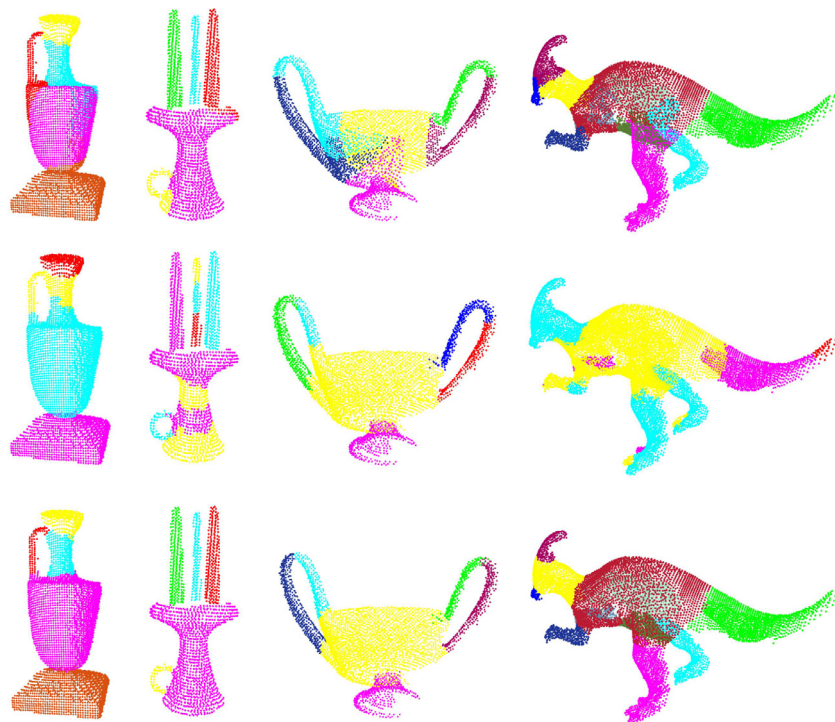


Fig. 12. Comparison of segmentation results with classical diffusion model(first row), WCSeg[7](second row) and our method (third row) for 3d point clouds.

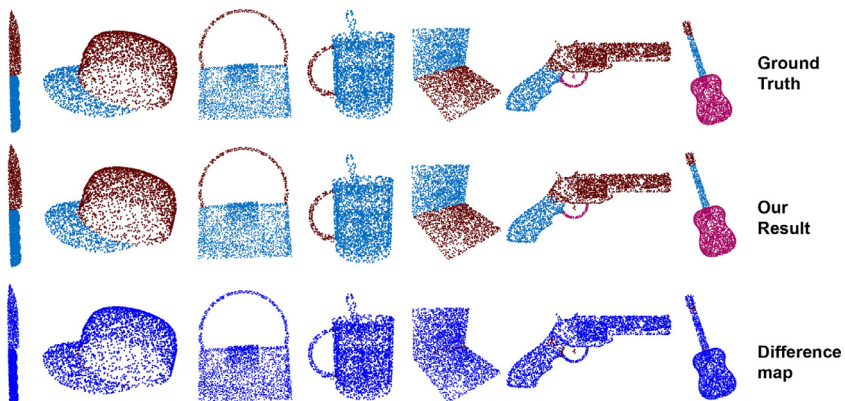


Fig. 13. Comparison of segmentation results between the ground-truth and our method. The ground-truth segmentations (used for training on Pointnet dataset[50]) are given in the first row. The segmentations by our algorithm are shown in the second row, and the difference maps are computed and shown in the third row(the red dots correspond to the different labeled points between the ground-truth and our results). (For interpretation of the references to colour in this figure legend, the reader is referred to the web version of this article.)

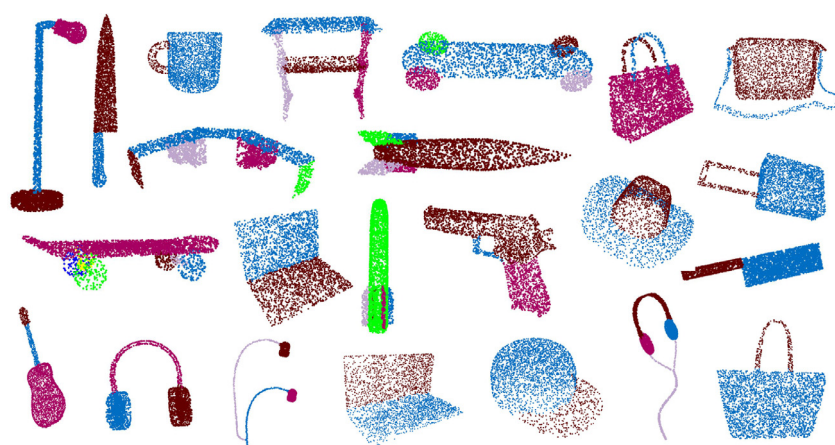


Fig. 14. Segmentation results with total variation diffusion model for Pointnet dataset[50].



Fig. 15. Segmentation results with total variation diffusion model for more 3d point clouds.

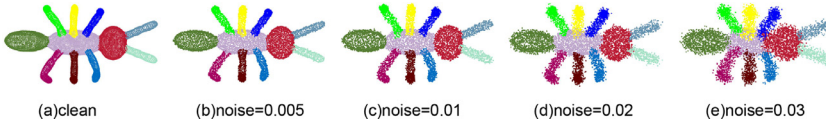


Fig. 16. Segmentation results by our method for data with noise at different levels.

ferent levels. As shown, for data with modest level noise, our algorithm can produce well segmentation results (see (a-d) in Fig. 16). However, when the noise is quite high, the segmentation boundaries are not well(see the yellow part of (e) in Fig. 16).

The above comparisons visually show that total variation diffusion model can generate better decomposition results than the classical diffusion model (1) and other several existing methods for both meshes and 3d point clouds. In the following, we further analyse our algorithm from the influences of initializations and quantitative numerical errors to show the stability. The following three metrics will be used to present the error curves of our algorithm.

5.4. Initialization and quantitative analysis for Algorithm 1

As our algorithm needs initializations, we analyze the influence of initializations on the algorithm. In addition, to demonstrate the stability of our algorithm, we also present the corresponding error curves according to the following three error metrics:

$$\Phi - \text{Metric} = \log(\|\Phi^k - \Phi^{k-1}\|^2)$$

$$\mathbf{q} - \text{Metric} = \log(\|\mathbf{q}^k - \nabla \Phi^k\|^2)$$

$$\mathbf{z} - \text{Metric} = \log(\|\mathbf{z}^k - \Phi^k\|^2)$$

As our algorithm is affected by the initializations, we acquire the initializations via the spectral clustering algorithm in [42](which is based on the facts: the eigenfunctions of Laplace operator are orthogonal, and the positions of max/min element of eigenfunctions of Laplace operator are scattered enough to approximate the initializations). Fig. 17 exhibits segmentation results with different initializations. As can be seen, when the initializations are scattered over each part of the data you would like to segment, our algorithm can produce good segmentation results (see (a) (computed via the clustering algorithm in [42]) and (b) (being a disturbance of (a))). On the contrary, when the initializations are not well-distributed, our algorithm can not get well results (see(c-e)). According to our test, for most data, the algorithm in [42] can provide well initializations. Moreover, in Fig. 18, we present segmentation results with different \mathbf{K} in Algorithm 1 for the same

Algorithm 1 ALM for solving shape segmentation problem (10)

1. Initialization:

- 1.1 $s_i, i = 1, 2, \dots, K$;
- 1.2 $\lambda^{-1} = 0, \mathbf{q}^{-1} = 0, \mathbf{z}^{-1} = 0, l = 0, \varepsilon = 10^{-5}$;

2. Repeat

- 2.1 For fixed $\mathbf{q}^{l-1}, \mathbf{z}^{l-1}$, computing Φ^l by (16);
- 2.2 For fixed Φ^l, \mathbf{z}^{l-1} , computing \mathbf{q}^l by (18);
- 2.3 For fixed Φ^l, \mathbf{q}^l , computing \mathbf{z}^l by (19);
- 2.4 Update Lagrange multiplier $\lambda_{\mathbf{q}}^l, \lambda_{\mathbf{z}}^l$:

$$\lambda_{\mathbf{q}}^l = \lambda_{\mathbf{q}}^{l-1} + r_{\mathbf{q}}(\mathbf{q}^l - \nabla_S \Phi^l), \quad \lambda_{\mathbf{z}}^l = \lambda_{\mathbf{z}}^{l-1} + r_{\mathbf{z}}(\mathbf{z}^l - \Phi^l)$$

3. Until($\|\Phi^l - \Phi^{l-1}\|^2 < \varepsilon$).

Table 2

The computational time for point clouds in Fig. 10 by Algorithm 1

Model	Vertex	SegNumber	Time(s)
Moon	2000	4	0.5
Light	7831	7	4
Jar	17836	6	31
Fish	10186	6	22

data, which show that our algorithm can perceive the segmentation boundaries effectively with different K .

Fig. 19 presents the error curves of our algorithm according to the above error metrics for results in Fig. 9, 10, which show that all the errors with respect to the iteration number decrease fastly. This also indicates that our algorithm is numerically robust.

5.5. Computational costs

We now discuss the computational costs. Overall, our algorithm is quite simple. The main step requiring CPU costs is solving the quadratic programming problem (16). Fortunately, the coefficient matrix keeps unchanged in our iterative algorithm. It can be pre-factored and thus the whole algorithm is quite efficient. In our tests, we note that the segmentation part K also affects the algorithm efficiency. The more the segmenting parts, the slower the algorithm is. Table. 2 presents the computational time for the re-

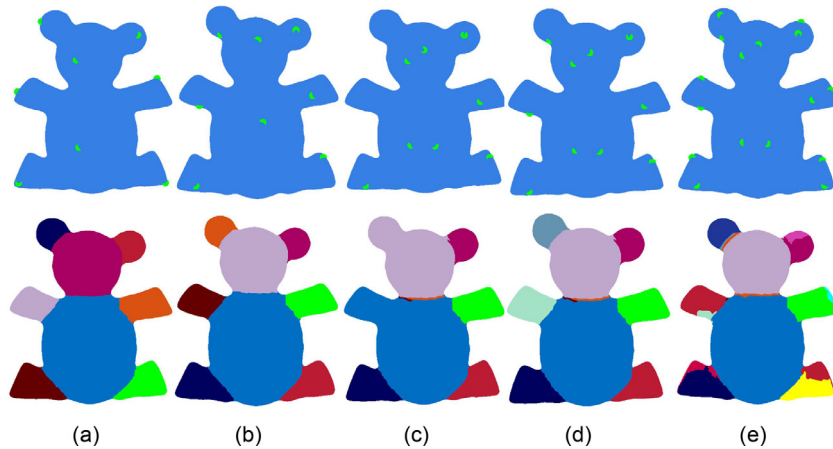


Fig. 17. Segmentation results with different initializations in [Algorithm 1](#). (a) initialization computed via [42], (b) is a disturbance of (a), (c-e) random selection.

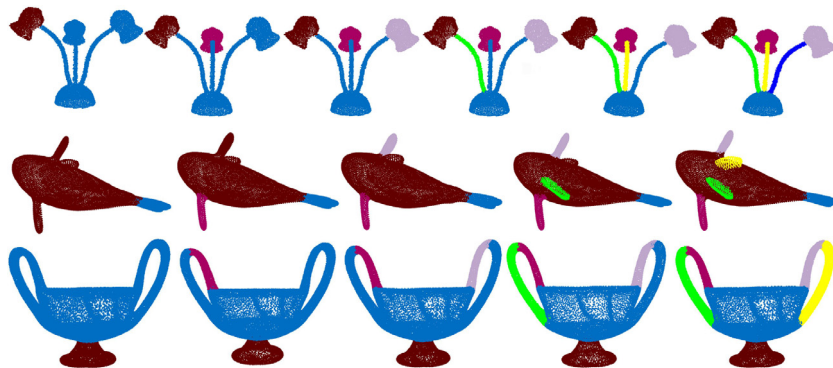


Fig. 18. Segmentation results with different K in [Algorithm 1](#) for point data. From left to right, the segmentation part K increases gradually.

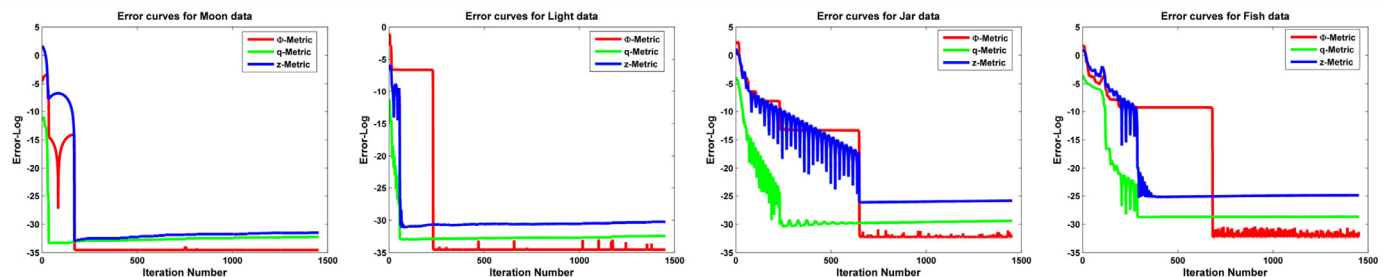


Fig. 19. The error curves of [Algorithm 1](#) for results in [Fig. 9, 10](#)

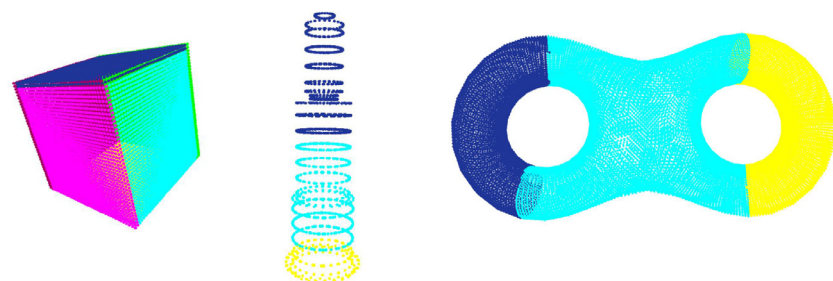


Fig. 20. Some failure results produced by our method

sults in Fig. 10 by Algorithm 1, which shows that our algorithm can achieve better results in reasonable costs.

5.6. Limitations

Our total variation diffusion model has been demonstrated effectively in producing edge-preserving segmentation results, but it still has some limitations. For example, we cannot acquire the number of segmentation parts automatically. In addition, for meshes with degenerated triangles, we cannot obtain the initializations accurately (which is based on the spectral clustering theory in [42]: the positions of max/min elements of eigenfunctions of Laplace operator). As far as we know, for clustering-based segmentation problem, it is an open problem to acquire the cluster centers. Besides, for point clouds with few features or not well-distributed, our method cannot produce satisfying results; see the results in Fig. 20.

6. Conclusion

Based on the good edge-preserving and sparsity property of total variation regularization, this paper introduces a novel diffusion model by minimizing weighted total-variation energy with Dirichlet boundary constraints. By this weighted total variation diffusion model, we propose a new shape segmentation optimization method, which is very simple and involving one stage to get the effective segmentation results. The optimization problem is solved effectively by augmented Lagrangian method with each subproblem having closed form solution. Plenty of experiments demonstrate that our total variation diffusion segmentation method can produce piecewise constant segmentation results with clear boundaries, both for meshes and point clouds. Furthermore, when compared with classical diffusion model and several existing segmentation methods including evaluated on the Princeton Mesh Segmentation Benchmark and pointnet data set, our method can produce better results than most of these methods, especially for shapes with sharp features. In addition, the quantitative errors show that the algorithm is robust numerically and the computational costs are reasonable.

There are a few problems for further investigation. For instance, skeleton extraction based on our total variation diffusion model will be reported in details subsequently.

Declaration of Competing Interest

The authors declare that they have no competing interests.

CRediT authorship contribution statement

Huayan Zhang: Methodology, Software, Validation, Investigation, Data curation, Writing - original draft, Visualization, Supervision, Funding acquisition. **Chunxue Wang:** Conceptualization, Formal analysis, Resources, Writing - review & editing, Project administration.

Acknowledgements

We would like to thank Noa Fish, Kalogerakis for providing their segmentation data of [7] and [8], the Princeton Segmentation Benchmark [2] and Pointnet [50]. This work was also supported by the NSF of China (Nos. 61802279, 61602341) and NSF of Tianjin(Nos. 18JCQNJC00100, 17JCQNJC00600).

References

- [1] Shamir A. A survey on mesh segmentation techniques. *Comput Graph Forum* 2008;27(6):1539–56.
- [2] Chen X, Golovinskiy A, Funkhouser T. A benchmark for 3d mesh segmentation. *ACM Trans Graph* 2006;66(5):1632–48.
- [3] Lavoué G, Dupont F, Baskurt A. A new cad mesh segmentation method, based on curvature tensor analysis. *Computer-Aided Design* 2005;37(10):975–87.
- [4] Golovinskiy A, Funkhouser T. Randomized cuts for 3d mesh analysis. *ACM Trans Graph* 2008;27(5).
- [5] Kalogerakis E, Hertzmann A, Singh K. Learning 3d mesh segmentation and labeling. *ACM Trans Graph* 2010;29(3).
- [6] Yan D, Wang W, Liu Y, Yang Z. Variational mesh segmentation via quadric surface fitting. *Computer-Aided Design* 2012;44(11):1072–82.
- [7] Kaick O, Fish N, Kleiman Y, Asafi S, Cohen-Or D. Shape segmentation by approximate convexity analysis. *ACM Trans Graph* 2014;34(1).
- [8] Kalogerakis E, Averkiou M, Maji S, Chaudhuri S. 3d shape segmentation with projective convolutional networks. In: CVPR; 2017. p. 3779–88.
- [9] Rodrigues RS, Morgado JF, Gomes AJ. Part-based mesh segmentation: A survey. In: Comput. Graph. Forum, vol. 37. Wiley Online Library; 2018. p. 235–74.
- [10] Belkin M, Sun J, Wang Y. Discrete laplace operator on meshed surfaces. In: Proceedings of the twenty-fourth annual symposium on Computational geometry. ACM; 2008. p. 278–87.
- [11] Meyer M, Desbrun M, Schröder P, Barr AH. Discrete differential-geometry operators for triangulated 2-manifolds. In: Visualization and mathematics III. Springer; 2003. p. 35–57.
- [12] Xu G. Discrete laplace–beltrami operators and their convergence. *Computer Aided Geometric Design* 2004;21(8):767–84.
- [13] Wu C, Deng J, Chen F, Tai X. Scale-space analysis of discrete filtering over arbitrary triangulated surfaces. *SIAM J Imaging Sci* 2009;2(2):670–709.
- [14] Li X, Xu G, Zhang YJ. Localized discrete laplace–beltrami operator over triangular mesh. *Computer Aided Geometric Design* 2015;39:67–82.
- [15] Weickert J. Anisotropic diffusion in image processing, vol. 1. Teubner Stuttgart; 1998.
- [16] Clarenz U, Diewald U, Rumpf M. Anisotropic geometric diffusion in surface processing. In: Proceedings of the conference on Visualization'00. IEEE Computer Society Press; 2000. p. 397–405.
- [17] Andreux M, Rodola E, Aubry M, Cremers D. Anisotropic laplace–beltrami operators for shape analysis. In: ECCV. Springer; 2014. p. 299–312.
- [18] Lindqvist P. Notes on the p-Laplace equation; 2017.
- [19] Pérez P, Gangnet M, Blake A. Poisson image editing. *ACM Trans Graph* 2003;22(3):313–18.
- [20] Lim JS. Two-dimensional signal and image processing. Englewood Cliffs, NJ, Prentice Hall; 1990, 710 p 1990.
- [21] Torkamani-Azar F, Tait K. Image recovery using the anisotropic diffusion equation. *IEEE Trans Image Process* 1996;5(11):1573–8.
- [22] Perona P, Malik J. Scale-space and edge detection using anisotropic diffusion. *IEEE Trans Pattern Anal Mach Intell* 1990;12(7):629–39.
- [23] Desbrun M, Meyer M, Schröder P, Barr A. Implicit fairing of irregular meshes using diffusion and curvature flow. *ACM Trans Graph* 1999;317–24.
- [24] Bajaj C, Xu G. Anisotropic diffusion of surfaces and functions on surfaces. *ACM Trans Graph* 2003;22(1):4–32.
- [25] Sorkine O, Cohen-Or D, Lipman Y, Alexa M, Rössl C, Seidel H-P. Laplacian surface editing. In: Proceedings of the 2004 Eurographics/ACM SIGGRAPH symposium on Geometry processing. ACM; 2004. p. 175–84.
- [26] Reuter M, Biasotti S, Giorgi D, Patane G, Spagnuolo M. Discrete laplace–beltrami operators for shape analysis and segmentation. *Comput Graph* 2009;33(3):381–90.
- [27] Vallet B, Lévy B. Spectral geometry processing with manifold harmonics. In: Comput. Graph. Forum, vol. 27. Wiley Online Library; 2008. p. 251–60.
- [28] Au OK-C, Tai C-L, Chu H-K, Cohen-Or D, Lee T-Y. Skeleton extraction by mesh contraction. In: ACM Trans. Graph., vol. 27. ACM; 2008. p. 44.
- [29] Lévy B, Zhang HR. Spectral mesh processing. In: ACM SIGGRAPH 2010 Courses. ACM; 2010. p. 8.
- [30] Song R, Liu Y, Martin RR, Rosin PL. Mesh saliency via spectral processing. *ACM Trans Graph* 2014;33(1):6.
- [31] Chahrou M, Moumouni L, Far ME, Gadi T. Segmentation of 3d meshes using p-spectral clustering. *IEEE Trans Pattern Anal Mach Intell* 2014;36(8):1687–1693.
- [32] Zheng Y, Tai C-L, Zhang E, Xu P. Pairwise harmonics for shape analysis. *IEEE Trans Vis Comput Graph* 2013;19(7):1172–84.
- [33] Sela M, Afalo Y, Kimmel R. Computational caricaturization of surfaces. *Computer Vision and Image Understanding* 2015;141:1–17.
- [34] Botsch M, Kobbelt L, Pauly M, Alliez P, Lévy B. Polygon Mesh Processing, vol. pp.250. CRC Press; 2010.
- [35] Liu R, Zhang H. Segmentation of 3d meshes through spectral clustering. In: Proceedings of the Pacific Conference on Computer Graphics and Applications; 2004. p. 298–305.
- [36] Attene M, Falciadino B, Spagnuolo M. Hierarchical mesh segmentation based on primitives. *The Vis Comput* 2006;22(3):181–93.
- [37] Liu R, Zhang H. Mesh segmentation via spectral embedding and contour analysis. *Comput Graph Forum* 2007:385–94.
- [38] Lai Y, Hu S, Martin R, Rosin P. Fast mesh segmentation using random walks. In: Proceedings of SPM; 2008. p. 183–91.
- [39] Au O, Zheng Y, Chen M, Xu P, Tai C. Mesh segmentation with concavity aware fields. *IEEE Trans Vis Comput Graph* 2012;18(7):1125–34.
- [40] Zhang J, Zheng J, Wu C, Cai J. Variational mesh decomposition. *ACM Trans Graph* 2012;31(3):21.
- [41] Zheng Y, Tai C, Wu OK-C. Dot scissor: A single-click interface for mesh segmentation. *IEEE Trans Vis Comput Graph* 2012;18(8):1304–12.

- [42] Zhang H, Wu C, Deng J, Liu Z, Yang Y. A new two-stage mesh surface segmentation method. *The Visual Computer* 2017;1–19.
- [43] Mumford D, Shah J. Optimal approximations by piecewise smooth functions and associated variational problems. *Commun Pur Appl Math* 1989;42(5):577–685.
- [44] Rudin LI, Osher S, Fatemi E. Nonlinear total variation based noise removal algorithms. *Physica D: nonlinear phenomena* 1992;60(1–4):259–68.
- [45] Chambolle A, Lions P-L. Image recovery via total variation minimization and related problems. *Numerische Mathematik* 1997;76(2):167–88.
- [46] Bredies K, Kunisch K, Pock T. Total generalized variation. *SIAM J Imag Sci* 2010;3(3):492–526.
- [47] Elsey M, Esego g lu S. Analogue of the total variation denoising model in the context of geometry processing. *Multiscale Modeling & Simulation* 2009;7(4):1549–73.
- [48] Wu C, Zhang J, Duan Y, Tai X. Augmented lagrangian method for total variation based image restoration and segmentation over triangulated surfaces. *J Sci Comput* 2012;50(1):145–66.
- [49] Zhang H, Wu C, Zhang J, Deng J. Variational mesh denoising using total variation and piecewise constant function space. *IEEE Trans Vis Comput Graph* 2015;21(7):873–86.
- [50] Qi CR, Su H, Mo K, Guibas LJ. Pointnet: Deep learning on point sets for 3d classification and segmentation. In: Proceedings of the IEEE conference on computer vision and pattern recognition; 2017. p. 652–60.
- [51] Michelot C. A finite algorithm for finding the projection of a point onto the canonical simplex of r^n . *J Optim Theory Appl* 1986;50(1):195–200.
- [52] Wu C, Tai X. Augmented lagrangian method, dual methods, and split bregman iteration for rof, vectorial tv, and high order models. *SIAM J Imaging Sci* 2010;3(3):300–39.
- [53] Shapira L, Shamir A, Cohen-Or D. Consistent mesh partitioning and skeletonisation using the shape diameter function. *The Vis Comput* 2008;24(4):249–59.
- [54] Nguyen A, Le B. 3d point cloud segmentation: A survey. In: 2013 6th IEEE conference on robotics, automation and mechatronics (RAM). IEEE; 2013. p. 225–30.
- [55] Vo A-V, Truong-Hong L, Laefer DF, Bertolotto M. Octree-based region growing for point cloud segmentation. *ISPRS Journal of Photogrammetry and Remote Sensing* 2015;104:88–100.
- [56] Rusu RB, Blodow N, Marton ZC, Beetz M. Close-range scene segmentation and reconstruction of 3d point cloud maps for mobile manipulation in domestic environments. In: 2009 IEEE/RSJ International Conference on Intelligent Robots and Systems. IEEE; 2009. p. 1–6.